Jet Noise Source Modification Due to Forward Flight

R. S. Larson,* C. J. McColgan,† and A. B. Packman‡
Pratt & Whitney Aircraft, East Hartford, Conn.

The effects of forward flight on the turbulence characteristics of a jet in a coflowing stream have been determined for a 2.22 in. circular jet in a 36 in. free jet wind tunnel. The nozzle exit velocity was 400 fps and the tunnel velocity was set at 0, 40, 120, and 200 fps. Measurements of flow properties including mean velocity, turbulence intensity and spectra, convection velocity, integral length scale, and convected frame integral time scale were carried out using two linearized hot wires. Results were used to predict changes due to flight in the jet acoustic sources. The noise reductions for a cold jet with a velocity of 1000 fps, due to the change in acoustic sources in flight, agreed well at all angles with measured noise reductions.

I. Introduction

EXTENSIVE use of noise-absorbing materials in the inlet and exhaust ducting of modern high bypass ratio turbofan engines has reduced the noise generated by fans, compressors, turbines, and burners to the level that the jet noise (noise generated in the exhaust plume by mixing the high velocity jet with the ambient air) is an important part of the total noise signature of current aircraft. The characteristics of jet noise from turbojet and turbofan engines have been well documented under static conditions. However, aircraft noise certification limits must be satisfied under actual aircraft flyover conditions during takeoff and approach operations. Thus, it is important that methods be developed to more accurately predict the jet noise under flight conditions.

The effect of flight on jet noise of a circular jet exhaust has been simulated by testing in wind tunnels.[1,2] Noise measurements obtained in wind tunnel tests show that the jet exhaust noise of nozzles operating subsonically is reduced in flight from the static levels at all measurement angles. However, noise measurements obtained from some flyover tests[3] have shown less noise reduction than the results of the wind tunnel tests. In order to help resolve the differences in wind tunnel and flyover results, it is necessary to understand the effects of flight on the fundamental mechanisms of jet noise generation. Measuring the changes caused by flight in the aerodynamic parameters responsible for noise generation and relating these changes to the measured noise reductions caused by flight will provide a more basic understanding of the effect of flight on jet noise than is currently available. This understanding will allow eventual improvements in our ability to develop more accurate in-flight predictions.

The noise reduction in flight is generally attributed to changes in the strength of the acoustic sources distributed throughout the jet shear layer. The acoustic source strength at a point in the jet shear layer is determined from the local aerodynamic flow properties. The mean and turbulence flow quantitites needed to determine the acoustic source strength are mean velocity, mixing layer growth, turbulence intensity, integral length scale, eddy convection velocity, and integral time scale corresponding to the eddy lifetime in a frame moving at the eddy convection velocity. Limited measurements of the changes in the shear layer of a jet in a wind tunnel flow have been used to predict the noise reduction in flight.[2] These attempts were unsuccessful, suggesting either that the reduction in noise may not be explained entirely on the basis of changes in the jet turbulence structure or that a more complete series of turbulence measurements is required. The present investigation was designed to provide a consistent set of data for the effect of flight on the jet shear layer characteristics and to predict, based on the shear layer measurements, the reduction in noise due to flight.

The turbulence characteristics of an axisymmetric jet in a static environment have been investigated in many studies.[4-6] The corresponding data for a jet in a coflowing stream are less comprehensive. In Refs. 7-9, the turbulence properties of a plane two-stream mixing layer were measured. However, such a mixing layer may not simulate the shear layer of an axisymmetric jet a coflowing stream. The mean velocity and turbulence intensity for an axisymmetric jet in a coflowing stream were determined in Refs. 10 and 11, but the other turbulence properties required for jet noise prediction, such as integral length scale, integral time scale, and eddy convection velocity, were not measured. An extensive set of data was obtained in Ref. 12 for a coaxial nozzle with an area ratio of 10, but the noise reductions expected on the basis of these measurements were not investigated. Furthermore, the structure of the inner shear layer of the coaxial nozzle would be affected by the developing outer shear layer at large downstream positions. Therefore, a complete set of data is not available for the turbulence and mean flow properties of a jet in a large area ratio wind tunnel.

The current investigation consisted of the measurement of the turbulence and mean flow properties of a jet in a coflowing stream and the prediction of the in-flight jet noise reduction using these measurements. The measurement apparatus is discussed in Sec. II and the flow measurements are presented in Sec. III. The predicted in-flight jet noise reduction based on the flow measurements is derived in Sec. IV and compared to the reductions obtained from acoustic measurements in Ref. 1. Concluding remarks are presented in Sec. V.

II. Experimental Procedure

Wind Tunnel Facility

The investigation was carried out in the United Technologies Research Center Acoustic Research Facility,[13] a free jet wind tunnel which provides an anechoic environment for flight simulation of aircraft and jet engine noise sources. Figure 1 is a schematic of the tunnel configuration. The fan and drive motor for the tunnel flow are downstream of the test section, while the model nozzle flow is provided by compressors. Adjustable louvers provide control of the tunnel velocity. Honeycomb and screens are located in the inlet and,

Presented as Paper 77-58 at the AIAA 15th Aerospace Sciences Meeting, Los Angeles, Calif., Jan. 24-26, 1977; submitted March 25, 1977; revision received Nov. 7, 1977.

Index categories: Aeroacoustics; Jets, Wakes, and Viscid-Inviscid Flow Interactions.

*Research Engineer, Jet Noise Technology Group. Member AIAA.
†Analytical Engineer, Jet Noise Technology Group.
‡Assistant Project Engineer, Jet Noise Technology Group.

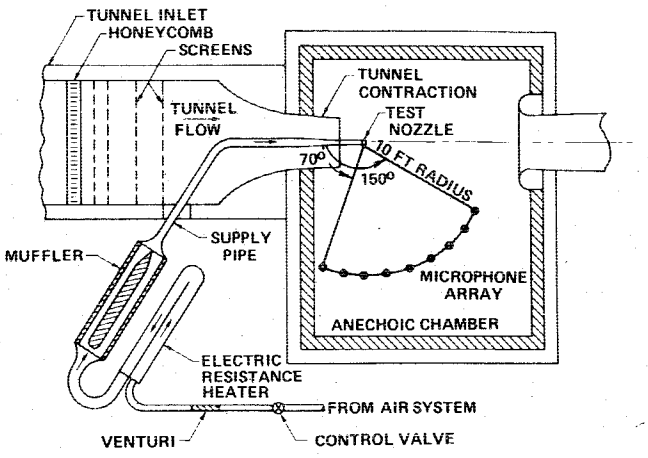

Fig. 1 UTRC acoustic research facility.

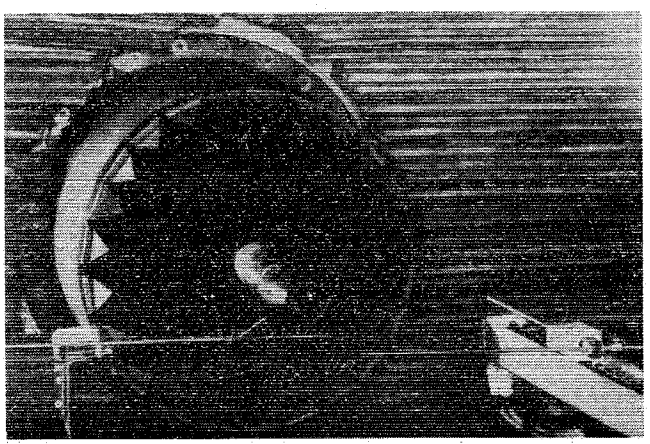

Fig. 2 Model nozzle and hot wire installation.

in conjunction with a contraction ratio of 11.5, provide a uniform low turbulence (0.12%) test section flow.

Figure 2 shows the test arrangement employed in this study. A round convergent nozzle with an exit diameter of 2.22 in. was positioned coaxially with the tunnel flow. The tunnel nozzle diameter is 36 in., resulting in a ratio of tunnel area to model nozzle area of 262. This large area ratio was sufficient to insure that the tunnel shear layer did not disturb the model nozzle flow in the region of interest.

The nozzle was operated at a nominal exit velocity of 400 fps, while the tunnel velocity was set at values of 0, 40, 120, and 200 fps. The resulting values of the velocity ratio, m, defined as the wind tunnel velocity divided by the jet velocity, were 0, 0.1, 0.3, and 0.5. Three downstream measurement stations, normalized by the jet diameter, D, were selected for each velocity ratio as shown in Table 1.

Data were taken at $x/D=3$ for all velocity ratios to provide measurements at a common point for direct comparison. The hot wire probes were moved downstream at the other stations to maintain approximately the same ratio of downstream distance to potential core length, since the potential core lengthens with increasing tunnel speed. For each axial measurement station three radial positions were established, denoted as the inner and outer "edges" of the shear layer and the "center." The edges were defined to be the points where the velocity fluctuation level was 50% of the peak level, and the center was defined as the peak fluctuation location. Convection velocity was the principal quantity determined at the edges. The nozzle and tunnel flow total pressures were set for a given temperature to give the desired velocities.

Table 1 Downstream measurement station locations

Velocity ratio, m	Axial measurement stations, x/D		
0	3	5	7
0.1	3	5.5	7.7
0.3	3	6.8	9.5
0.5	3	7.7	12.1

Hot Wire Measurements

Hot wire measurements of local flow properties were made at each of the stations in Table 1. The hot wire measurements were divided into two categories, according to whether a single probe or two probes were necessary to acquire the data. A single probe was used to measure mean velocity and turbulence intensity profiles, and its signal was analyzed to provide frequency spectra and autocorrelations for selected points in the shear layer. The signals from two probes were cross correlated for varying values of probe separation. Longitudinal convection velocities, integral length scales, and integral time scales were determined from the cross correlation records. The probes were mounted on traverse mechanisms. The upstream probe, A, traversed radially, while the downstream probe, B, traversed axially along the jet.

Thermo-Systems, Inc. model 1210-T1.5 standard hot wire probes were used in conjunction with model 1054A anemometers for the data acquisition. The sensors were 1.3 mm long and 0.004 mm in diameter, and the probes were operated in the constant temperature mode. The anemometer bridge outputs were linearized to simplify data analysis. The signals from both probes were bandpass filtered from 0-20 kHz to remove a spurious electrical resonance in the frequency range of 200-500 kHz. At 20 kHz the spectrum levels were 30 dB lower than the levels at the spectrum peak frequency. At the beginning of each test run, the voltage output of each anemometer was calibrated against flow velocity with the individual probe in the potential core of the jet (as in Ref. 5), and the resulting calibrations were used to reduce the data.

Single-Probe Measurements

The mean and fluctuating voltage signals (which were proportional to mean and fluctuating velocities) from probe A were read from a digital dc voltmeter and rms ac voltmeter, respectively, as the probe was radially stepped across the jet flow. Narrowband frequency spectra were obtained at the radial position of maximum fluctuation intensity using a Spectral Dynamics 301C spectrum analyzer and 302C ensemble averager.

Two-Probe Measurements

The two-probe measurements were used to determine the local turbulence convection velocity, integral length scale, and integral time scale. Autocorrelations and cross correlations were obtained using a Saicor model SAI-42 probability and

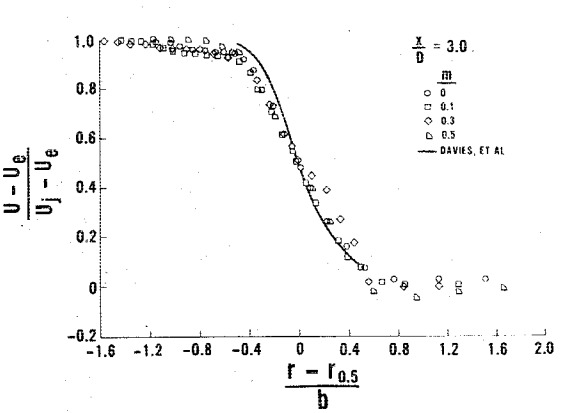

Fig. 3 Normalized mean velocity profiles.

cross-properties analyzer. Cross correlations at each axial station in Table 1 were obtained for 12 different probe separations. The cross correlations were normalized by the autocorrelations to give the normalized cross correlation coefficient defined as

$$R_{AB}(x_A,x_B,\tau)=\frac{\overline{u'(x_A,t)u'(x_B,t+\tau)}}{\sqrt{u'(x_A,t)^2u'(x_B,t)^2}} \quad (1)$$

where an overbar indicates a time average, and τ is the time delay between the signals from probe A and probe B.

III. Results of the Flow Investigation

Single-Probe Measurements

Mean Velocity

Figure 3 is a plot of normalized mean velocity vs normalized radius. The normalized velocity, $\hat{U}$, is defined as

$$\hat{U}=(U-U_e)/(U_j-U_e)$$

where U is the local mean velocity, U_j is the jet velocity, and U_e is the tunnel flow velocity. The normalized radius, $\hat{r}$, is defined as

$$\hat{r}=(r-r_{0.5})/b$$

where $\hat{r}_{0.5}$ is the radial position at which $\hat{U}=0.5$ and b is the mixing layer width based on 5% boundaries (defined in the next section). The data collapse well and agree well with the normalized static jet data of Ref. 5. The negative normalized velocity near the edges of the jet, at a normalized radius of +1.0, is a residual effect due to the external boundary layer of the nozzle due to the external flow. The external boundary layer thickness normalized by the nozzle diameter increased as velocity ratio increased to a value of 0.54 for a velocity ratio of 0.5.

Mixing Layer Growth

The mixing layer width b is defined as the distance between the locations where the normalized velocity is 0.95 and 0.05, or

$$b=r_{0.95}-r_{0.05}$$

The mixing layer was found to grow linearly with downstream distance. The effect of external velocity on mixing layer width is shown in Fig. 4. The data collapse, using a least-squares fit, to the line given by

$$\sqrt{\frac{1+m}{1-m}}\,\frac{b}{D}=0.24+0.13\,\frac{x}{D} \quad (2)$$

The inverse of the variation of the mixing layer width, b, with relative velocity was used as an approximation to the variation of the potential core length with relative velocity. This approximation is not exact because the mixing layer width does not develop symmetrically with respect to the nozzle lip. However, the difference is small and will be neglected in the analysis of Sec. IV.

Turbulence Intensity.

Peak turbulence intensity at an axial station of $x/D=3.0$ was found to decrease with increasing flight speed as shown in Fig. 5. The reduction is represented by the line

$$u_p'/u_{p\,|m=0}'=(1-m)^{0.7} \quad (3)$$

where u_p' is the peak fluctuating velocity component at a given x/D. The exponent 0.7 was also determined in Ref. 10 for several velocity ratios and axial stations. This would imply that the value of the exponent 0.7 is not sensitive to small differences in the experimental apparatus because the data were taken in different facilities. Differences between the facilities include 1) different turbulence levels in the potential core of the nozzles and 2) different boundary layer thicknesses on the outside of the nozzle. The turbulence level in the nozzle potential core in the present experiment was approximately 1.5%, while the corresponding level from Ref. 10 was 2.5%. The initial boundary layer thickness of the flow around the nozzle, normalized by the nozzle diameter, was 0.31 for the facility in Ref. 10 and was 0.54 for the present investigation (for a velocity ratio, m, of 0.5 in both cases).

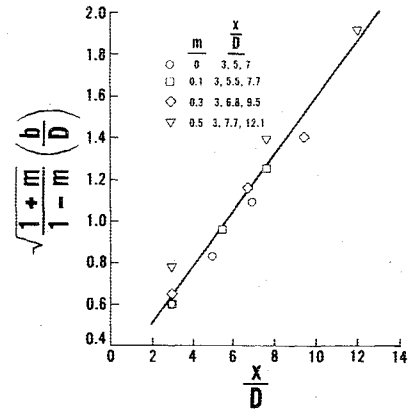

Fig. 4 Mixing layer growth.

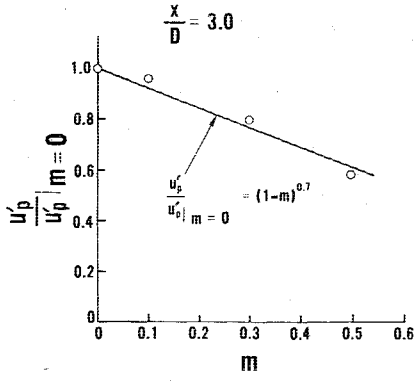

Fig. 5 Reduction of peak turbulence intensity with velocity ratio.

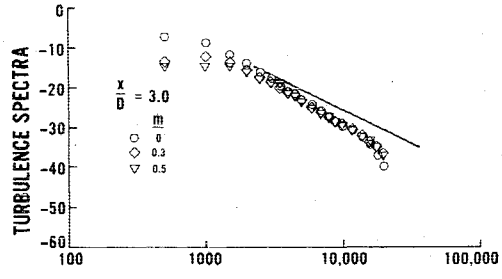

Fig. 6 Effect of velocity ratio on turbulence spectra.

Turbulence Spectra

Turbulence spectra were obtained by analyzing the fluctuating anemometer output with the Spectral Dynamics spectrum analyzer and ensemble averager. The turbulence spectrum was defined as the narrowband analysis (with a constant bandwidth of 78 Hz) of the fluctuating anemometer output. Figure 6 shows the effect of increasing velocity ratio on the frequency content of the turbulence. The spectra were obtained in the peak turbulence region of the shear layer. At a given axial station, the low frequency content decreases as

forward flight velocity increases, but the levels at high frequencies remain constant. This suggestes that flight effects do not change the turbulence microscale associated with the high frequency levels but do affect the large scale eddies associated with the low frequency levels.

A line representing the $-5/3$ power law is also shown in Fig. 6. While the data are close to this law, the slope is actually found to be -2.04. This is in very good agreement with the results of previous experimenters who show values of -2.07, -2.09, and -2.08 (Refs. 4, 12, and 7, respectively).

Two-Probe Measurements

Convection Velocity

The convection velocity was determined by cross correlating the fluctuating signals of two hot wires which were separated axially by a distance Δx. Convection velocities were calculated by dividing the separation Δx by the time delay for the maximum cross correlation coefficient. A more precise calculation of convection velocity is described in Ref. 5. However, the more simple procedure used here results in answers within 4% of the exact method. With one probe fixed at a given measurement station, convection velocities were calculated for two separation distances of the two probes. Convection velocities for the two axial separations agreed within 10%. The normalized convection velocity, U_c, was defined as

$$\hat{U}_c = (U_c - U_e)/U_j - U_e$$

where U_c is the measured convection velocity.

The normalized convection velocity at the radial station of maximum turbulence intensity is shown plotted against the axial position in Fig. 7. Included is a line, $\hat{U}_c = 0.57$, which is the average of the values shown on the plot. The average normalized correction velocity in the peak turbulence region of the shear layer, 0.57, is approximately the same as the value 0.50 obtained in Ref. 5 for a circular nozzle in a static environment and 0.52 obtained in Ref. 8 for a two-dimensional mixing layer.

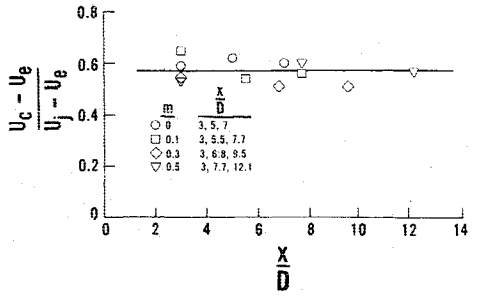

Fig. 7 Normalized convection velocity in the peak turbulence region of the shear layer as a function of x/D.

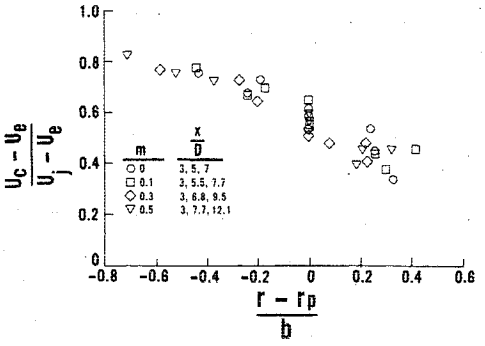

Fig. 8 Radial variation of normalized convection velocity.

Convection velocity varies across the shear layer much more slowly than the mean velocity. The normalized convection velocity is plotted in Fig. 8 against a normalized radius for all velocity ratios and axial positions. The convection velocity decreases from a maximum value of about 0.85 at the inner edge of the shear layer to about 0.45 at the outer edge of the shear layer, whereas from Fig. 3, the mean velocity decreases from a maximum of 0.95 to about 0.20 toward the outer edge of the shear layer.

Integral Length Scale

The integral length scale is a measure of the distance over which the turbulence remains correlated. If Δx is defined as the separation distance between hot wire probes A and B, the axial integral length scale, L, is defined by

$$L = \int_0^\infty R_{AB}(\Delta x, \tau = 0)\, d(\Delta x) \tag{4}$$

When R_{AB} contains negative lobes it is customary to integrate only to the first zero crossing. The axial length scales in the peak turbulence region of the shear layer for all velocity ratios and axial stations are plotted vs the corresponding mixing layer width in Fig. 9. The data collapse in Fig. 9 shows that the length scale is proportional to the mixing layer width for all velocity ratios. That is, the axial variation of the integral length scale is the same as that for the mixing layer width. The data are represented by the line

$$L = 0.29b \tag{5}$$

Cross correlations $R_{AB}(\Delta x, \tau = 0)$ were plotted vs $\Delta x/L$ in Fig. 10. The resulting collapse of the cross-correlation curves shows that the cross correlation at zero time delay is a function only of probe separation divided by the integral length scale.

The constant in Eq. (5) depends upon the definition used to determine the mixing layer width. For example, in Ref. 11 a definition which produced smaller mixing layer widths was used and the proportionality constant in Eq. (5) was con-

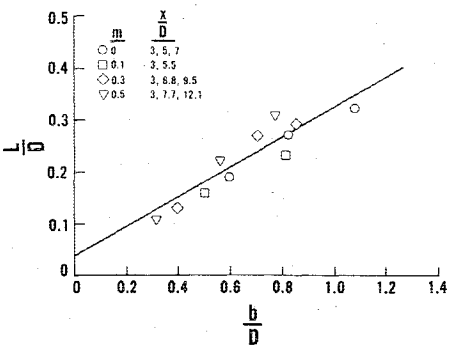

Fig. 9 Fixed frame integral length scale in the peak turbulence region of the jet shear layer.

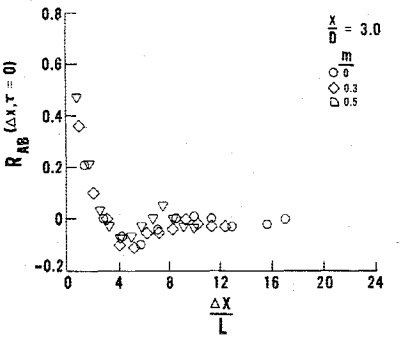

Fig. 10 Axial cross correlation at zero time delay in the peak turbulence region of the jet shear layer.

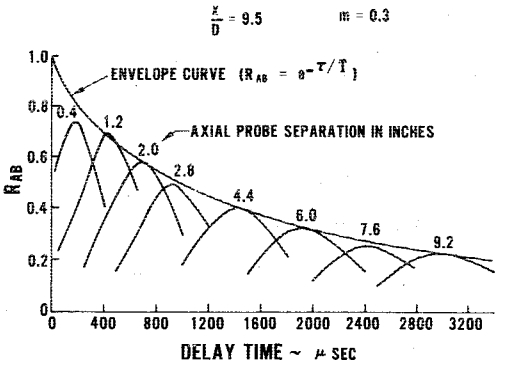

Fig. 11 Space-time cross correlations in the peak turbulence region of the jet shear layer.

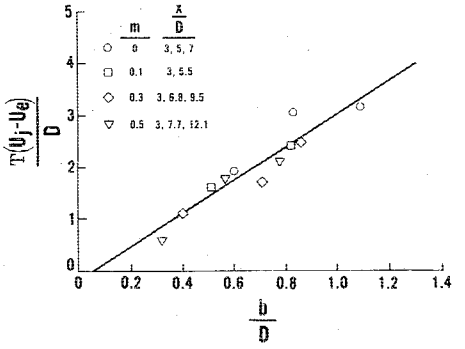

Fig. 12 Convected frame integral time scale in the peak turbulence region of the jet shear layer.

sequently larger. The same constant, 0.29, may be calculated from the results in Refs. 7 and 8 for a two-dimensional mixing layer with the same definition of mixing layer width used herein.

Integral Time Scale

The integral time scale in a coordinate frame moving at the local turbulence convection velocity is defined by the autocorrelation curve in the convected frame. The autocorrelation in the convected frame is determined by plotting $R_{AB}(X_A, X_B, \tau)$ as a function of time delay for different axial separations as indicated in Fig. 11. The envelope tangent to each curve is then the autocorrelation function in the convected frame of reference. If a curve of the form

$$R_{AB} = e^{-\tau/T} \tag{6}$$

is fit to the envelope autocorrelation curve, the integral time scale in the convected frame of reference is defined by the value of T required to give a best fit to the envelope curve. A close approximation of T was determined by plotting the peaks of the cross correlation curves in Fig. 11 vs time delay and fitting Eq. (6) to this curve. The calculated integral length scales in the peak turbulence region of the jet shear layer were found to be proportional to the mixing layer width divided by the relative velocity between the jet and external flow as illustrated in Fig. 12. The data are represented by the line

$$T = 3.17b/(U_j - U_e) \tag{7}$$

The small offset from the origin of the line in Fig. 12 is due to the virtual origin of the nozzle flow.

Equation (7) is valid for all axial measurement positions. Figure 13 contains normalized convected frame autocorrelations plotted as a function of τ/T. The collapse of the autocorrelation curves indicates that in the convected frame of reference the autocorrelation is a function only of

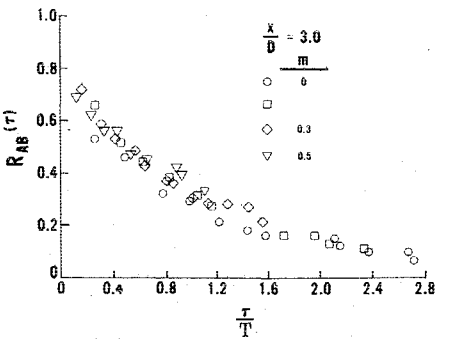

Fig. 13 Convected frame autocorrelations in the peak turbulence region of the jet shear layer.

time delay divided by integral length scale. Equation (7) shows that the integral time scale is proportional to the mixing layer width divided by the relative velocity between the jet and coflowing stream or, equivalently, inversely proportional to the mean shear. This result illustrates the necessity of using jets in a coflowing stream to obtain turbulence measurements rather than a $2D$ mixing layer. For example, it was determined in Ref. 8 that the proportionality constant in Eq. (7) for a $2D$ mixing layer differs from that for a static round jet. The proportionality constant in Eq. (7) is consistent with the result for a coaxial jet obtained in Ref. 12.

Equations (5) and (7) and the relation $U_c \cong \frac{1}{2}(U_j + U_e)$ may be combined to determine the ratio of the characteristic turbulence eddy size to the distance an eddy travels (in a reference frame fixed with respect to the flow). This ratio, denoted by α, is

$$\alpha = L/[(U_c - U_e)T] = 0.18 \tag{8}$$

Therefore, α is independent of all flow properties. The quantity α is used in the convective amplification factor for quadrupole sources in the jet shear layer to account for the finite existence of a turbulent eddy.

Summary of Turbulence Properties

General scaling laws for the turbulence characteristics of a round jet in a free jet wind tunnel have been determined in this investigation and are summarized in Table 2.

The properties summarized in Table 2 are in basic agreement with those obtained in Ref. 12 for the inner shear layer of a coaxial jet. The integral time scale and mixing layer growth relations in Table 2 differ from the corresponding relations for a two-dimensional mixing layer while the convection velocity and integral length scale relations are similar. Since these results were obtained for a relatively low velocity cold jet, they may require modification for hot, high velocity, or supersonic jets.

Table 2 Scaling laws for turbulence properties

Convection velocity	$U_c \cong \frac{1}{2}(U_j + U_e)$
Mixing layer growth	$\frac{\sqrt{1+m}}{1-m}\frac{b}{D} = 0.24 + 0.13\frac{x}{D}$
Integral length scale	$L = 0.29b$
Integral time scale	$T = 3.17\frac{b}{U_j - U_e}$
Peak turbulence	$\frac{u'_p}{u'_p\|_{m=0}} = (1-m)^{0.7}$
Alpha	$\alpha = 0.18$

IV. Jet Noise Reduction with Forward Flight

The turbulence measurements described in Sec. III may be used to calculate the flight reduction in noise based on the change due to flight in the jet noise sources. These calculated reductions will be compared to the noise reductions measured in the same facility.[1] The noise data in Ref. 1 were obtained for jets with high velocity (1000-1670 fps) over a range of temperatures from 300°F to 900°F, while the flow measurements discussed in Sec. III were obtained for an unheated flow. Consequently, the comparison of the noise reductions in flight predicted from the turbulence measurements with the measured noise reductions will focus on low temperature jets. Comparisons are also shown for high temperature jets in which it is assumed that the flow measurements are valid at high temperature.

Definition of Acoustic Source Strength

Overall sound pressure level (OASPL) may be written, according to the form of Lighthill theory,[14] as

$$\mathrm{OASPL} \propto 10\log\left[\frac{\int_V \overline{u'^2_R} f^4 v_e \mathrm{d}V}{[(1-M_c\cos\theta)^2+(\alpha M_c)^2]^{5/2}}\frac{1}{R^2}\right] \quad (9)$$

where $\overline{u'^2_R}$ is the turbulence component in the (R,θ) direction, f is a characteristic frequency, v_e is the characteristic volume of a turbulent eddy, V is the noise-generating volume of the jet, M_c is the eddy velocity relative to the external flow divided by the ambient speed of sound, θ is an observation angle measured with respect to the downstream jet axis, and R is the distance from the observer to the jet. It will be assumed that all turbulence components vary with relative velocity in the same manner as the axial turbulence component and the quantity $\overline{u'^2_R}$ will be replaced with the axial turbulence component $\overline{u'^2}$.

Equation (9) may be rewritten as

$$\mathrm{OASPL} \propto 10\log\left(\frac{Q}{[(1-M_c\cos\theta)^2+(\alpha M_c)^2]^{5/2}}\frac{1}{R^2}\right) \quad (10)$$

in which the acoustic source strength, defined as Q, has been separated from the convective amplification. Convective amplification is due to the relative motion between the sources, medium, and observer. The acoustic source strength Q is defined as

$$Q=\int \overline{u'^2}^2 f^4 v_e \mathrm{d}V \quad (11)$$

Q may be expressed in terms of the turbulence properties in Sec. III. For example, the frequency of noise generated by a turbulent eddy is inversely proportional to the integral time scale. That is, $f \propto T^{-1}$.

The volume of an eddy is proportional to the integral length scale cubed, or $v_e \propto L^3$.

Finally, the element of $\mathrm{d}V$ of the noise-producing region of the jet shear layer may be written

$$\mathrm{d}V \cong \pi b D \mathrm{d}x$$

Equation (11) may, therefore, be integrated since all functions in the integrand have been determined in Sec. III as a function of axial position. The result is

$$Q=c\int_0^{\ell} \overline{u'^2}^2 T^4 L^3 b D \mathrm{d}x \quad (12)$$

where c is a constant and ℓ is the length of the potential core of the jet. All quantities in Eq. (12) are evaluated only in the peak turbulence region of the shear layer.

Relation of Static and Flight OASPL

Specific relations for OASPL similar to Eq. (11) may be written for static and forward flight simulation experiments. Static OASPL, denoted $\mathrm{OASPL_{STA}}$, may be written

$$\mathrm{OASPL_{STA}} \propto \log\left(\frac{Q_{\mathrm{STA}}}{[(1-M_c\cos\theta)^2+(\alpha M_c)^2]^{5/2}}\frac{1}{R^2}\right) \quad (13)$$

where Q_{STA} is the static acoustic source strength.

In a wind tunnel forward flight simulation experiment, if data are corrected to account for the convection of sound by the wind tunnel flow (see Refs. 1 or 2), the analog to Eq. (13) is

$$\mathrm{OASPL_{SIM}} \propto \log\left\{\frac{Q_{\mathrm{SIM}}}{1+M_e\cos\theta}\frac{1}{R^2} \times \frac{1}{[(1-(M_c-M_e)\cos\theta)^2+(\alpha(M_c-M_e))^2]^{5/2}}\right\} \quad (14)$$

where M_e is the Mach number of the external flow relative to the ambient speed of sound and Q_{SIM} is the acoustic strength in flight. Q_{SIM} and Q_{STA} may be related by using the scaling laws from Table 2 in Eq. (12). The variation in length of the potential core with flight is assumed to be inverse of the variation of the mixing layer width, as described in Sec. III. The relation between Q_{SIM} and Q_{STA} is then

$$Q_{\mathrm{SIM}}=(1-m)^{5.8}\sqrt{1+m}\,Q_{\mathrm{STA}} \quad (15)$$

$\mathrm{OASPL_{STA}}$ and $\mathrm{OASPL_{SIM}}$ are therefore related by

$$\mathrm{OASPL_{SIM}}=\mathrm{OASPL_{STA}}+10\log\left(\frac{(1-m)^{5.8}\sqrt{1+m}}{1+M_e\cos\theta} \times \frac{[(1-M_c\cos\theta)^2+(\alpha M_c)^2]^{5/2}}{[(1-(M_c-M_e)\cos\theta)^2+(\alpha(M_c-M_e))^2]^{5/2}}\right) \quad (16)$$

Relative Velocity Exponents

In Ref. 1, the effects of forward flight on jet noise were determined experimentally in the same acoustic wind tunnel used for the present aerodynamic measurements. The noise reductions in flight determined in this experiment were summarized by the use of exponents defined as

$$n=\frac{\mathrm{OASPL_{STA}}-\mathrm{OASPL_{SIM}}}{10\log[U_j/(U_j-U_e)]} \quad (17)$$

The jet operating conditions used in Ref. 1 were primarily high-temperature, high-velocity conditions.

An expression of the exponent in terms of the measured turbulence properties can be obtained by substituting Eq. (16) into Eq. (17). The result is

$$n=\log\left\{\frac{(1-m)^{5.8}\sqrt{1+m}}{1+M_e\cos\theta} \times \frac{[(1-M_c\cos\theta)^2+(\alpha M_c)^2]^{5/2}}{[(1-(M_c-M_e)\cos\theta)^2+(\alpha(M_c-M_e))^2]^{5/2}}\right\} \div \log\frac{U_j-U_e}{U_j} \quad (18)$$

Since all quantities in Eq. (18) were determined in Sec. III, exponents may be calculated from Eq. (18) and compared with those determined experimentally in Ref. 1. All terms in Eq. (18) are a function of relative velocity and jet velocity except for the factor $(1+M_e\cos\theta)$. If $\mathrm{OASPL_{SIM}}$ data are corrected for this factor, the exponent at a given velocity

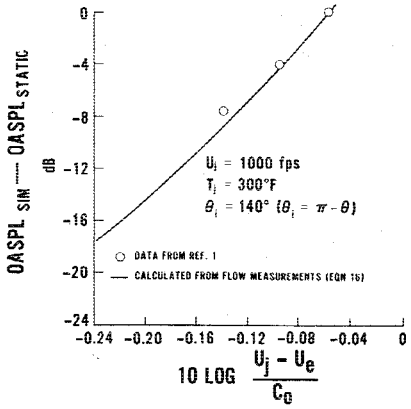

Fig. 14 Relative velocity effect on OASPL.

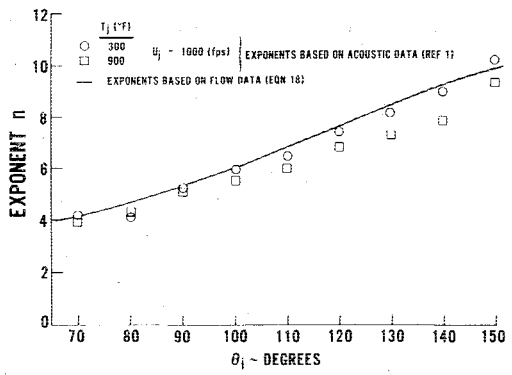

Fig. 15 Relative velocity exponents as a function of angle.

should be only a function of relative velocity. The exponents in Ref. 1 contain the factor $(1+M_c\cos\theta)$, and this factor was retained in Eq. (18) in calculating exponents.

Comparison of the exponents calculated from Eq. (18) and exponents measured in Ref. 1 are contained in Figs. 14-16. Figure 14 illustrates the effect of flight on OASPL at a fixed angle (140 deg with respect to the upstream jet axis) for a jet velocity of 1000 fps and temperature of 300°F. The calculated reduction in level with increasing flight speed, using Eqs. (17) and (18), is in good agreement with the experimentally measured noise reductions from Ref. 1. The calculated exponent also varies linearly with $\log[(U_j-U_e)/c_0]$ which is in agreement with experimental results. Figure 15 contains calculated exponents for a jet velocity of 1000 fps plotted as a function of the angle θ_i, which is measured with respect to the upstream jet axis ($\theta_i=\pi-\theta$). Experimentally determined exponents using the results from Ref. 1 are shown for a jet velocity of 1000 fps with temperatures of 300°F and 900°F. The agreement between the calculated exponents from the turbulence measurements and the exponents from Ref. 1 is good for the jet flow at 300°F. The measured exponents from Ref. 1 decrease with increasing jet temperature, which implies that the scaling relations for the turbulence and mean flow properties determined in Sec. III may be altered for jets at high temperatures. Alternatively, increased refraction of sound generated within the shear layer by the temperature gradient may be the cause of the experimental variation with temperature.

Figure 16 contains exponents for jet velocities of 1000, 1200, and 1670 fps at a temperature of 900°F. The exponents from the turbulence measurements are larger at aft angles than the experimental exponents from Ref. 1, although the correct qualitative behavior of the calculated exponents (including a crossover at forward angles) is observed. As jet velocity and temperature are increased the discrepancy between the two sets of exponents also increases. This effect may be a result of increased refraction of sound by the velocity gradient as jet velocity was increased. The increase in

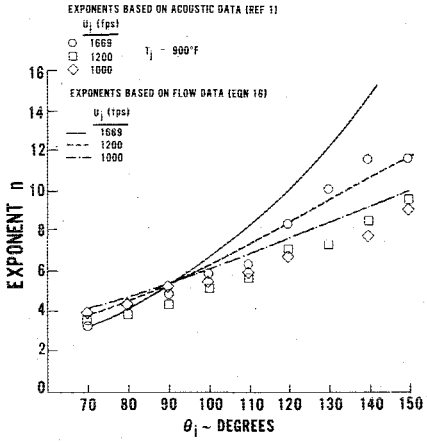

Fig. 16 Variation of relative velocity exponents with jet velocity.

exponents as jet temperature decreases, illustrated in Fig. 15, suggests that exponents obtained from noise measurements at the same velocities, but lower temperature, would agree better with the calculated exponents.

The exponents in Figs. 15 and 16 calculated from Eq. (18) collapse to a value of approximately 4.5 at 90 deg and agree with the exponents calculated from the acoustic data in Ref. 1. The reduction in noise at 90 deg with relative velocity arises from the reduction in the acoustic source strength of sources in the jet shear layer.

Figures 14 and 15 indicate that the jet noise reductions observed in forward flight simulation experiments at low temperatures and velocities may be explained on the basis of reductions in the acoustic source strength in the jet shear layer and reductions in convective amplification. At higher velocities and temperatures, the difference between calculated and experimental exponents indicates that the turbulence scaling laws determined in Sec. III may change as velocity and temperature increase. The extension of the calculated exponents to these flows would require turbulence, mean velocity, and mean temperature measurements in high-velocity, high-temperature flows.

V. Concluding Remarks

1) General scaling laws for the mean velocity, turbulence intensity, convective amplification, integral length scale, and integral time scale have been determined for a low velocity incompressible jet in a coflowing stream.

2) The turbulence measurements were used to determine the change in acoustic source strength of sources in the jet shear layer due to flight and the change in kinematic factors such as convective amplification due to flight. Relative velocity exponents calculated from the changes in acoustic source strength and convective amplification due to flight were compared to relative velocity exponents obtained from jet noise measurements. Agreement between the calculated and experimental exponents was good for low-velocity, low-temperature jets.

3) At high velocities and temperatures, the calculated exponents were larger than the measured exponents which suggests that the turbulence scaling relations determined in the low-velocity, unheated jet may be modified for high-velocity and high-temperature flows.

4) Measurements of mean flow and turbulence properties in high-velocity, high-temperature flows with a laser-velocimeter could be used to extend the calculated exponents into the high-velocity, high-temperature regime.

Acknowledgment

Part of the shear layer properties in this report were obtained under NASA Contract NAS3-17866, "Acoustic Tests of DBTF Jet Noise Simulation."

References

[1] Packman, A. B., Ng, K. W., and Paterson, R. W., "Effect of Simulated Forward Flight on Subsonic Jet Noise," *Journal of Aircraft*, Vol. 13, Dec. 1976, pp. 1007-1013.

[2] Cocking, B. J. and Bryce, W. D., "Subsonic Jet Noise in Flight Based on Some Recent Wind-Tunnel Results," AIAA Paper 75-462, 1975.

[3] Bushell, K. W., "Measurements and Prediction of Jet Noise in Flight," AIAA Paper 75-461, 1975; also AIAA *Progress in Astronautics and Aeronautics—Aeroacoustics: Jet Noise, Combustion and Core Engine Noise*, Vol. 43, edited by I. R. Schwartz, New York, 1976, pp. 137-158.

[4] Laurence, J., "Intensity, Scale, and Spectra of Turbulence in the Mixing Region of a Free Subsonic Jet," NACA Rept. 1292, 1956.

[5] Davies, P.O.A.L., Fisher, M. J., and Barratt, M. J., "The Characteristics of the Turbulence in the Mixing Region of a Round Jet," *Journal of Fluid Mechanics*, Vol. 15, 1963, pp. 337-367.

[6] Nayer, B. M., Siddon, T. E., and Chu, W. T., "Properties of the Turbulence in the Transition Region of a Round Jet," University of Toronto Institute for Aerospace Studies Tech. Note No. 131, 1969.

[7] Spencer, B. W. and Jones, B. G., "Statistical Investigation of Pressure and Velocity Fields in the Turbulent Two-Stream Mixing Layer," AIAA Paper 71-613, 1971.

[8] Jones, B. G., Planchon, H. P., and Hammersley, R. J., "Turbulent Spacetime Correlation Measurements in a Plane Two-Stream Mixing Layer at Velocity Ratio 0.3," AIAA Paper 73-225, 1973.

[9] Wygnanski, I. and Fiedler, H. E., "The Two Dimensional Mixing Region," JEM 41, 1970, pp. 327-361.

[10] Plumblee, H. E., ed., "A Study of the Effects of Forward Flight on Turbulent Jet Mixing Noise," Final Report for NASA Contract NAS3-18540, Lockheed-Georgia.

[11] Morris, P. J., "Turbulence Measurements in Subsonic and Supersonic Axisymmetric Jets in a Parallel Stream," *AIAA Journal*, Vol. 14, Oct. 1976, pp. 1468-1475.

[12] deBelleval, J., Leuchter, F. O., and Perulli, M., "Simulation of Flight Effects on the Structure of Jet Mixing Layers for Acoustic Applications," AIAA Paper 76-559, 1976.

[13] Paterson, R. W., Vogt, P. G., and Foley, W. M., "Design and Development of the United Aircraft Reseach Laboratories Acoustic Research Tunnel," *Journal of Aircraft*, Vol. 10, July 1973, p. 427.

[14] Proudman, I., "The Generation of Noise by Isotropic Turbulence," Proceedings of the Royal Society of London, A214, 1952, pp. 119-132.